

ADGaussian: Generalizable Gaussian Splatting for Autonomous Driving with Multi-modal Inputs

Qi Song¹, Chenghong Li¹, Haotong Lin², Sida Peng², Rui Huang^{1#}

¹The Chinese University of Hong Kong, Shenzhen ²Zhejiang University

{qisong, chenghongli}@link.cuhk.edu.cn, {haotong1, pengside}@zju.edu.cn, ruihuang@cuhk.edu.cn

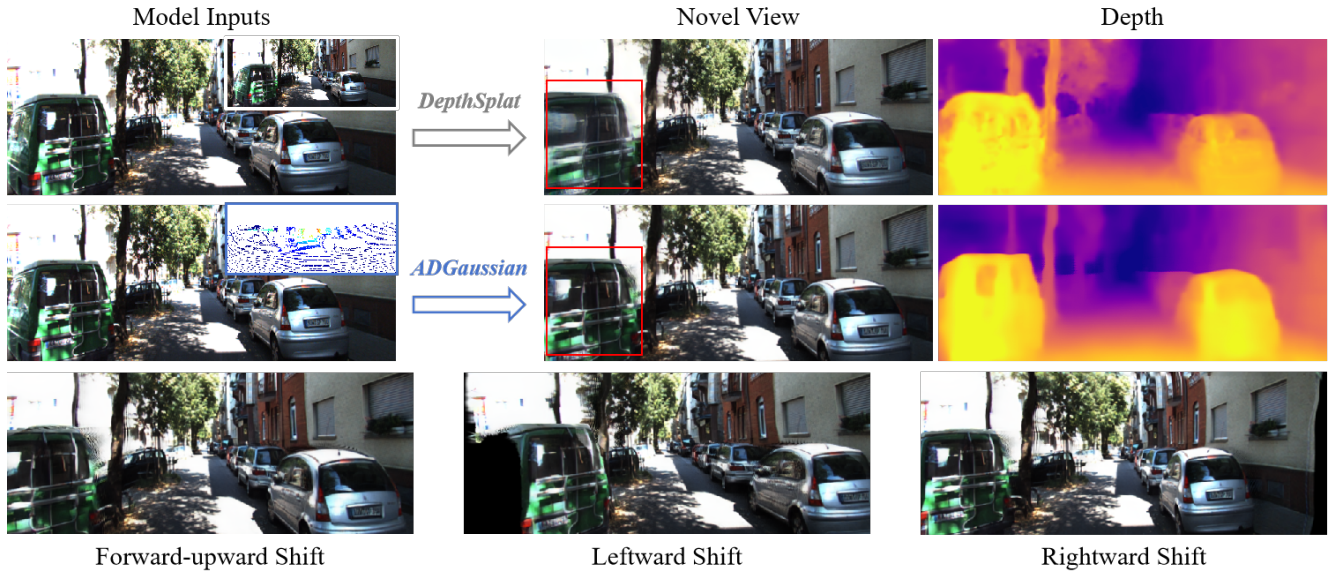


Figure 1. We introduce **ADGaussian**, a generalizable Gaussian framework for street scene reconstruction. Our approach achieves superior performance in both visual and geometric reconstruction. The bottom row illustrates the results of viewpoint shifting, further demonstrating the robustness of our method under varying viewpoint changes.

Abstract

We present a novel approach, termed *ADGaussian*, for generalizable street scene reconstruction. The proposed method enables high-quality rendering from single-view input. Unlike prior Gaussian Splatting methods that primarily focus on geometry refinement, we emphasize the importance of joint optimization of image and depth features for accurate Gaussian prediction. To this end, we first incorporate sparse LiDAR depth as an additional input modality, formulating the Gaussian prediction process as a joint learning framework of visual information and geometric clue. Furthermore, we propose a multi-modal feature matching strategy coupled with a multi-scale Gaussian decoding model to enhance the joint refinement of multi-modal features, thereby enabling efficient multi-modal Gaussian learning. Extensive experiments on two large-scale au-

tonomous driving datasets, *Waymo* and *KITTI*, demonstrate that our *ADGaussian* achieves state-of-the-art performance and exhibits superior zero-shot generalization capabilities in novel-view shifting. The project page can be found at maggiesong7.github.io/research/ADGaussian/.

1. Introduction

Recently, 3D Gaussian Splatting (3DGS) [14] has garnered significant attention in the fields of 3D scene reconstruction and novel view synthesis due to its real-time rendering speed and high-quality output. One key application is the modeling of street scenes from image sequences, which plays a vital role in areas such as autonomous driving.

When modeling urban scenes, some methods follow per-scene optimization techniques [4, 17, 48], notably *StreetGaussians* [38] that represents dynamic urban street as a

set of point clouds equipped with semantic logits and 3D Gaussians. While per-scene optimization approach excels in high-quality reconstruction, it often struggles with expensive training cost and large-range novel view synthesis.

To achieve generalizable street scene reconstruction, most existing methods build upon the architectures of PixelSplat [3] or MVSplat [6]. For instance, GGRT [19] introduces a pose-free architecture to iteratively update multi-view depth map and subsequently estimates Gaussian primitives based on PixelSplat. Similarly, GGS [9] enhances the depth estimations of MVSplat by integrating a multi-view depth refinement module. Nevertheless, multi-view feature matching-based depth estimation may fail in challenging conditions such as texture-less areas, and reflective surfaces. To tackle this issue, the concurrent work DepthSplat [36] combines pre-trained depth features from Depth Anything V2 [40] with multi-view depth estimations for accurate depth regression, where the estimated depth features are further used for Gaussian prediction.

Given the great generalization capability of Depth Anything V2, it is reasonable to extend DepthSplat to urban street scenarios. However, DepthSplat faces specific limitations when applied to these environments. First, the visual rendering quality is constrained by the effectiveness of pre-trained depth models. Additionally, even in cases where depth quality is high, straightforwardly concatenating image and depth features for Gaussian prediction leads to unsatisfactory visual reconstruction in complex autonomous driving situations (see Figure 1).

To this end, we propose a novel multi-modal representation framework aimed at enhancing both geometry modeling and visual rendering in street scenes. This framework leverages two complementary modalities: image visual cues and depth geometry clues. The key insight is to facilitate effective information sharing and joint optimization between different modalities. Specifically, our framework begins by integrating sparse LiDAR depth information as an additional input modality, which provides precise metric scale priors for enhanced geometry reconstruction. Given the image data and sparse depth map, we introduce an effective multi-modal feature matching strategy achieved by a Siamese-style encoder paired with an information cross-attention decoder. This design ensures a cohesive fusion of geometric and appearance information, resulting in well-aligned multi-modal tokens. Subsequently, we employ a multi-scale gaussian decoding model to aggregate multi-scale depth information into both image and depth tokens for the final Gaussian predictions. Notably, our model exhibits superior performance even under large viewpoint changes, as shown in the bottom row of Figure 1. This capability demonstrates the effectiveness of jointly optimizing multi-modal features, which enables superior geometry and texture reconstruction.

Overall, this work makes the following contributions:

- We present ADGaussian, the first generalizable framework that models street scenes using multi-modal data, specifically color images and depth maps.
- We develop a multi-modal feature matching strategy along with a multi-scale gaussian decoding model to facilitate effective multi-modal gaussian learning.
- We perform extensive comparisons on two large-scale driving datasets, showcasing our approach’s state-of-the-art performance and demonstrating the effectiveness of the proposed components.

2. Related Work

2.1. Generalizable 3D Gaussian Splatting

Generalizable Gaussian Splatting [5, 11, 32, 34, 37, 43] aims to learn powerful priors that enable effective generalization across unseen scenes. Existing methods can be broadly categorized into two groups. The first group, including approaches like PixelSplat [3], MVSplat [6], MVS-Gaussian [20], and SplatterImage [26], predicts per-pixel 3D Gaussian primitives using known camera parameters. The second group of methods [13, 23, 28, 41] proposes to jointly predict camera parameters and 3D representations, eliminating the need for known camera poses. For instance, GGRT [19] employs an Iterative Pose Optimization Network to estimate and iteratively update the relative pose between target and reference images. In street scene modeling, however, camera poses provide critical constraints for determining scene scale and enhancing reconstruction accuracy from video sequences. Moreover, camera poses are readily accessible in street scenes, making them a practical and reliable data resource. Therefore, we choose to leverage posed images for our approach.

2.2. Depth and Gaussian Splatting

Depth quality has been demonstrated to play a pivotal role in Gaussian Splatting. To ensure accurate geometry reconstruction, methods such as GPS-Gaussian [47] and DN-Splatter [29] incorporate additional depth supervision into the optimization process. However, as dense ground truth depth data is often unavailable, an alternative research direction has emerged, leveraging pre-trained depth foundation models [21, 40] to provide reliable geometric cues. For example, Chung et al. [7] rescale pre-trained depth maps using sparse COLMAP points, thereby offering accurate depth constraints for model optimization. Additionally, Flash3D [25] utilizes a frozen off-the-shelf network to estimate the metric depth, which subsequently serves as a direct input to the reconstruction model. To mitigate error propagation, DepthSplat [36] fuses pre-trained depth features with multi-view cost volume features while keeping the pre-trained network learnable. In contrast to previous

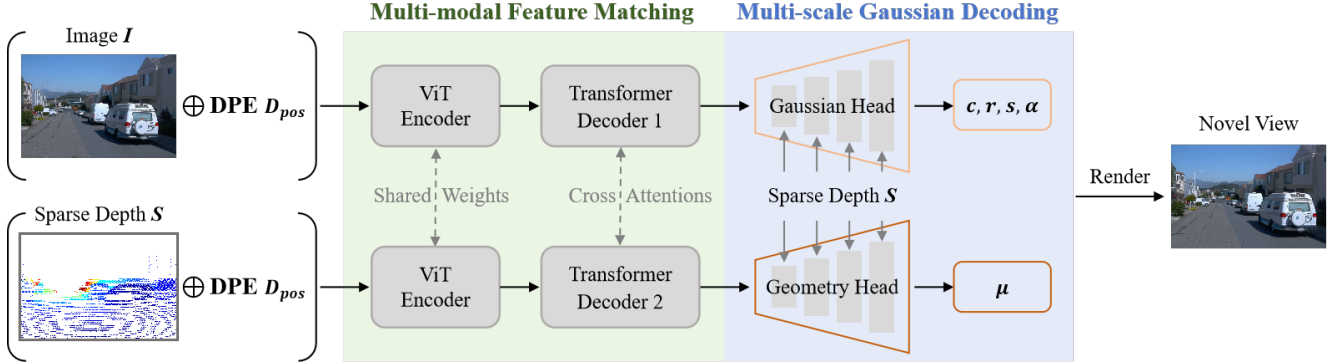


Figure 2. **Overview of ADGaussian.** Given monocular posed image with sparse depth as input, we first extract well-fused multi-modal features through Multi-modal Feature Matching, which contains a siamese-style encoder and a cross-attention decoder enhanced by Depth-guided positional embedding (DPE). Subsequently, the Gaussian Head and Geometry Head, augmented with Multi-scale Gaussian Decoding, are utilized to predict different Gaussian parameters.

approaches that focus primarily on geometry improvement, we argue that joint optimization of image and depth features is more critical for achieving high-quality reconstruction.

2.3. LiDAR-Integrated Gaussian Splatting

The integration of LiDAR data has emerged as a widely adopted approach in street scene reconstruction, mainly due to its effectiveness in facilitating geometry learning. The conventional methodologies typically involve two main steps: initializing Gaussians from LiDAR point clouds [15], and further supervising predicted Gaussian positions using LiDAR priors [4, 10, 12, 49]. However, reconstruction quality often degrades in areas where LiDAR measurements are unavailable. To address this limitation, HGS-Mapping [35] extracts matching feature points from adjacent RGB frames and utilizes the estimated spatial positions to initialize areas beyond LiDAR’s coverage. In the same manner, TCLCGS [46] constructs a hybrid 3D representation by combining LiDAR geometries with image colors, enabling simultaneous initialization of both geometric and appearance attributes of 3D Gaussians. Rather than directly using LiDAR point clouds, we propose leveraging sparse LiDAR depth to bridge the gap between LiDAR and camera data. Furthermore, we integrate depth priors into the training process, achieving joint optimization of depth geometries and image photometric attributes, as opposed to the common practice of initialization alone.

3. Methods

Depth foundation models [1, 2, 39, 40, 42] have been integrated into the Gaussian Splatting to improve geometry reconstruction. However, such framework often suffer from suboptimal rendering quality due to the insufficient interactions between photometric and geometric clues. To address this, we propose ADGaussian, a synchronized multi-modal

optimization architecture that combines sparse depth data with monocular images for enhanced street scene modeling.

3.1. Preliminary: Depth Foundation Model for Gaussian Splatting

Recently, works like DepthSplat have investigated the advantages of using a pre-trained depth foundation model for image-conditioned 3D Gaussian reconstruction, capitalizing on its remarkable performance across a variety of real-world datasets. All these methods utilize the pre-trained monocular depth features to augment the final depth estimation, thereby improving the quality of Gaussian rendering.

For instance, DepthSplat processes multi-view images $\{I^i\}_{i=1}^N (I \in \mathbb{R}^{H \times W \times 3})$ using two parallel branches to extract dense per-pixel depth. One branch focuses on modeling cost volume features C^i from the multi-view input, while the other employs a pre-trained monocular depth backbone, specifically Depth Anything V2, to obtain monocular depth features F_{mono}^i . Subsequently, the per-view cost volumes and monocular depth features are concatenated for 3D Gaussian prediction.

Intuitively, such models can be easily adapted to urban scenes. Nonetheless, we observed that the effectiveness of reconstruction is heavily dependent on the performance of the pre-trained depth foundation models, resulting in inconsistent accuracy across different street datasets and scenarios. Furthermore, the processing of image and depth features always occurs in parallel for each view, without any information sharing or synchronized optimization, which constrains the model’s learning capacity.

3.2. Multi-modal Feature Matching

In this section, we seek to find an effective way to integrate sparse LiDAR depth into Gaussian Splatting with full utilization of multi-modal features. To this end, we pro-

pose a *Multi-modal Feature Matching* architecture tailored for urban scenarios to enable the synchronous integration of sparse depth information and color image data. Throughout this process, *Depth-guided Position Embedding* incorporates depth cues into the position embedding, enhancing 3D spatial awareness and improving multi-modal contextual comprehension.

Multi-modal feature matching. As illustrated in Figure 2, at the core of our model is the *Multi-modal Feature Matching* of photometric features from the image and geometric cues from depth data. This is achieved through a Siamese-style encoder and an information cross-attention decoder, inspired by the DUS_t3R series [18, 30].

Specifically, a monocular image $I \in \mathbb{R}^{H \times W \times 3}$ and a synchronized sparse depth map $S \in \mathbb{R}^{H \times W}$ are fed into a weight-sharing ViT encoder in a Siamese configuration, resulting in two token representations F_I and F_S :

$$F_I = \text{Encoder}(I), F_S = \text{Encoder}(S). \quad (1)$$

The two identical encoders collaboratively process multi-modal features in a weight-sharing manner, allowing for the automatic learning of similarity characteristics.

After that, the transformer decoders equipped with cross attentions are employed to enhance information sharing and synchronized optimization between the two multi-modal branches. This step is crucial for producing well-fused multi-modal feature maps:

$$\begin{aligned} G_I &= \text{Decoder}_1(F_I, F_S), \\ G_S &= \text{Decoder}_2(F_S, F_I). \end{aligned} \quad (2)$$

Depth-guided positional embedding (DPE). The conventional positional embedding in Vision Transformers encodes either relative or absolute spatial positions on a 2D image plane to ensure spatial awareness within the image. However, relying solely on the geometric properties of a 2D image plane is insufficient for our synchronized multi-modal design. To this end, we propose a straightforward depth-guided positional embedding (DPE) to integrate depth positions with image-based spatial positions.

Specifically, given the downsampled image size $H_L \times W_L$ and the sparse depth map, we first flatten the 2D grid of spatial positions into a 1D vector, where each element corresponds to a specific spatial location in the image. Subsequently, the sparse depth map is downsampled to match the image resolution, generating an independent set of depth indices that complement the spatial positions. The final positional embedding D_{pos} is constructed by concatenating the flattened spatial positions with the depth positions, effectively encoding position information in the xy - z plane. By integrating both spatial and depth geometry, this module provides a comprehensive positional prior for effective multi-modal feature matching.

3.3. Multi-scale Gaussian Decoding

Given the multi-modal tokens G_I and G_S , our objective is to predict pixel-aligned Gaussian parameters $\{(\mu, \alpha, \Sigma, c)\}^{H \times W}$, where μ , α , Σ , and c are the 3D Gaussian’s center position, opacity, covariance, and color information. To fully leverage appearance cues and the geometry priors provided by image token G_I and depth token G_S , we implement two separate regression heads with the same architecture, namely Gaussian Head and Geometry Head, to generate different Gaussian parameters.

The two regression heads adhere to the DPT [22] architecture, enhanced with an additional multi-scale depth encoding that delivers precise scale priors for Gaussian prediction. In particular, at each scale within the DPT Decoder, we initially resize the input sparse depth map to align with the spatial size of the current feature scale. After that, the resized depth map is processed through a shallow network comprising two convolutional layers to extract depth features, which are then added to the DPT intermediate features. Finally, the input image and depth map, each processed by a single convolutional layer, are individually incorporated into the final features of the Gaussian Head and Geometry Head to facilitate either appearance-based or geometry-based Gaussian decoding.

3.4. Training Loss

Our model is trained using a combination of view synthesis loss and depth loss. The overall loss function is defined as follows:

$$\mathcal{L} = \mathcal{L}_{\text{nvs}} + \mathcal{L}_{\text{depth}} \quad (3)$$

Novel view synthesis loss. We train our full model with a combination of mean squared error (MSE) and LPIPS losses between rendered and ground truth image colors:

$$\mathcal{L}_{\text{nvs}} = \text{MSE}(I_{\text{pred}}, I_{\text{gt}}) + \lambda \cdot \text{LPIPS}(I_{\text{pred}}, I_{\text{gt}}) \quad (4)$$

where the LPIPS loss weight λ is set to 0.05.

Depth loss. We leverage depth loss to smooth the depth values of neighboring pixels, thereby minimizing abrupt changes over small regions:

$$\mathcal{L}_{\text{depth}} = \frac{1}{n} \sum_{i=1}^n \left(\frac{dD_i}{dx} e^{-\frac{dI_i}{dx}} + \frac{dD_i}{dy} e^{-\frac{dI_i}{dy}} \right) \quad (5)$$

where $\frac{dD_i}{dx}$, $\frac{dD_i}{dy}$, $\frac{dI_i}{dx}$, and $\frac{dI_i}{dy}$ denote the first derivatives of depth and image in the x and y -axis directions, respectively.

4. Experiments

4.1. Implementation Details

Datasets. We evaluate our proposed approach on two widely used autonomous driving datasets: the Waymo Open

Scene	PSNR \uparrow			SSIM \uparrow			LPIPS \downarrow			
	MVSplat [6]	DepthSplat [36]	Ours	MVSplat [6]	DepthSplat [36]	Ours	MVSplat [6]	DepthSplat [36]	Ours	
Static	003	21.79	19.99	31.09	0.679	0.627	0.931	0.143	0.192	0.059
	069	24.79	25.67	31.17	0.729	0.748	0.923	0.143	0.136	0.073
	232	28.79	26.76	30.52	0.873	0.819	0.904	0.077	0.094	0.083
	495	28.09	26.49	31.21	0.884	0.819	0.929	0.086	0.106	0.056
Dynamic	016	24.16	24.30	27.16	0.678	0.746	0.875	0.137	0.173	0.092
	021	19.58	18.42	19.61	0.636	0.619	0.659	0.243	0.316	0.273
	080	25.37	24.19	27.18	0.765	0.759	0.873	0.116	0.169	0.085
	096	21.55	21.67	21.46	0.684	0.680	0.691	0.250	0.264	0.263

Table 1. **Quantitative comparison with state of the art on Waymo dataset.** Our ADGaussian outperforms existing methods in nearly all scenarios. Cells highlighted in denotes the best and second-best performances.

Method	PSNR \uparrow	SSIM \uparrow	LPIPS \downarrow
MVSplat [6]	23.52	0.760	0.152
DepthSplat [36]	21.99	0.715	0.173
Ours	23.60	0.776	0.164

Table 2. **Quantitative comparison with state of the art on KITTI dataset.** Cells highlighted in denotes the best and second-best performances. Despite the inherent challenges posed by KITTI’s lower image quality and poor color reproduction, our method achieves a small but meaningful improvement over existing approaches using only single-frame image.

Dataset [24] and the KITTI Tracking benchmarks [8]. For both datasets, we adopt a train-test split ratio of approximately 1:7. Specifically, on the Waymo dataset, our focus primarily lies on static and dynamic scenes, where each scene type is divided into 4 test scenes and 28 training scenes. Similarly, for the KITTI dataset, the split consists of 5 test scenes and 37 training scenes. This partitioning ensures a balanced evaluation of our method across diverse scenarios, while also providing sufficient training data for effective model training.

Metrics. For render quality evaluation, we employ the standard image quality metrics, including Peak Signal-to-Noise Ratio (PSNR), Structural Similarity Index Measure (SSIM) [33], and the Learned Perceptual Image Patch Similarity (LPIPS) [44]. The running time and GPU memory usage are also provided to enable a comprehensive comparison of the trade-offs between speed and accuracy (see Supplementary Material for details).

Training details. Our implementation is based on the PyTorch framework. We employ the Adam [16] optimizer and cosine learning rate schedule, with an initial learning rate of $1e - 4$. We train our model on 3090 Ti GPUs, running for 150k iterations on both Waymo and KITTI datasets, with a batch size of 1. To ensure a fair comparison, all experiments are carried out at resolutions of 320×480 for the Waymo

dataset and 256×608 for the KITTI dataset.

4.2. Comparisons with the State of the Art

When comparing our work to the current state-of-the-art Gaussian Splatting methods, we have opted for the multi-view cost volume-based method, MVSplat [6], and the depth foundation model-based method, DepthSplat [36]. As GGRt [19] features a pose-free architecture, we excluded it from our comparisons. In each scenario, MVSplat and DepthSplat utilize two frames as input to generate subsequent novel frame for evaluation.

The quantitative comparisons on the Waymo and KITTI benchmarks are presented in Table 1 and Table 2, respectively. On the Waymo dataset, our ADGaussian surpasses previous state-of-the-art models on almost all visual metrics, with particularly notable improvements in static scenes. Additionally, our approach demonstrates consistent performance across diverse scenarios, underscoring the robustness of its multi-modal feature matching capabilities. From Table 2, it can be observed that the performance gain of our method on the KITTI dataset is less pronounced compared to that on the Waymo dataset. This is primarily attributed to the overall lower image quality and poor color reproduction of the KITTI dataset. Since our method relies solely on a single image as input, it retains fewer image details compared to previous works, which further constrains its performance on datasets with inferior image quality.

We also provide qualitative comparisons of the two datasets in Figure 3 and Figure 4. As can be seen, our model achieves superior rendering quality, particularly in occluded regions and fine details like slender signal poles.

Furthermore, the comparison between DepthSplat and MVSplat shows that DepthSplat exhibits stronger depth inference capabilities, attributed to its enhanced geometry reconstruction facilitated by pre-trained depth models. However, DepthSplat falls short in overall visual reconstruction quality due to its insufficient integration of appearance attributes, which is consistent with our earlier analysis in the preceding sections.



Figure 3. **Qualitative comparison with state of the art on Waymo dataset.** Our ADGaussian surpasses all other competitive models in rendering quality within urban scenarios, thanks to the efficacy of our multi-modal matching-based architecture.

4.3. Ablations and Analysis

Ablations on proposed components. The ablation studies are detailed in Table 3 to further confirm the efficacy of the proposed components. First, it can be seen that the full model achieves the highest performance, boasting a PSNR, SSIM, and LPIPS score of 31.0, 0.921, and 0.068, respectively. Notably, the removal of the depth-guided positional embedding (DPE) resulted in a decrease across all metrics (0.69, 1.3%, and 1%, respectively), emphasizing the significance of depth cues in facilitating the joint optimization of multi-modal features. Furthermore, the model lacking multi-scale Gaussian decoding (w/o Multi-scale) exhibited reduced performance, achieving a PSNR of 28.73, an SSIM of 0.868, and an LPIPS of 0.100, underscoring the effectiveness of multi-level depth decoding and independent Gaussian inference. Removing both DPE and Multi-scale led to a more substantial drop in performance, notably a 4.6% decrease in the LPIPS score.

Finally, to showcase the effectiveness of our synchronized multi-modal optimization formulation, we present the results without multi-modal feature matching (w/o Matching) by substituting the sparse depth input with a color image from the subsequent frame. It is evident that multi-modal feature matching brought about significant enhancement in PSNR, NDS, and mAP (4.32, 10.7%, and 3.8%,

Setup	PSNR \uparrow	SSIM \uparrow	LPIPS \downarrow
Full Model	31.00	0.921	0.068
w/o DPE	30.31	0.908	0.078
w/o Multi-scale	28.73	0.868	0.100
w/o DPE & Multi-scale	27.81	0.846	0.114
w/o Matching	26.68	0.814	0.106

Table 3. **Ablation studies on the Waymo dataset.** We report the averaged scores across all validation scenes for a more intuitive reflection of the model performance. The “Full Model” denotes our final model and all other ablation models are based on the final model by removing the mentioned module.

respectively), highlighting the importance of information exchange and synchronized optimization of image-related appearance features and depth-related geometric features.

Analysis on multi-modal inputs. To ensure a fair comparison, we constructed baseline networks with identical multi-modal inputs using state-of-the-art depth completion methods [31, 45]. Specifically, we re-implemented CFormer [45] and BpNet [27] as the comparison targets, which take both depth and image as inputs and predict Gaussian parameters using multi-modal fused features. As shown in Table 4, it is evident that the inclusion of addi-



Figure 4. **Qualitative comparison with state of the art on KITTI dataset.** As highlighted by the red boxes, our ADGaussian demonstrates superior performance in preserving visual consistency, particularly in handling fine details such as thin poles and object edges.

Method	PSNR \uparrow	SSIM \uparrow	LPIPS \downarrow
CFormer* [45]	25.71	0.796	0.126
BPNet* [27]	26.10	0.802	0.144
Ours	31.00	0.921	0.068

Table 4. **Performance analysis on multi-modal inputs.** Models marked with "*" are modified with a Gaussian head for 3DGS prediction. Despite utilizing multi-modal inputs, depth completion networks still suffer from the unsatisfactory novel view rendering quality, emphasizing the importance of joint optimization and collaborative prediction strategies.

tional depth input alone does not significantly enhance the quality of novel view rendering, further highlighting the critical need for our joint optimization. Moreover, the depth comparison results in Figure 5 reveal that our model excels in capturing fine-grained details, such as preserving the shape of cars and poles, even without pre-training on depth completion task. Additional details can be found in the Supplementary Material.

Cross-dataset generalization. We perform cross-dataset evaluation to demonstrate the generalization capability of our method to out-of-distribution novel scenes. Specifically, models trained on the KITTI dataset are directly evaluated on the Waymo dataset without fine-tuning. As shown in Table 5, even with only single-view input images, our

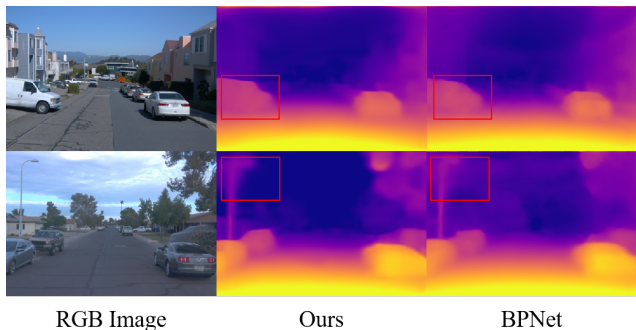


Figure 5. **Depth comparison with BPNet.** Our method demonstrates superior depth estimation performance in certain challenging regions, even without depth pre-training.

ADGaussian method consistently outperforms DepthSplat and achieves comparable cross-dataset generalization performance to MV+Splat, attaining higher PSNR and SSIM scores. This result underscores our robustness in handling diverse and unseen scenarios.

4.4. Application: Novel-view Shifting

The concept of novel-view shifting involves generating images from significantly varied perspectives compared to the original viewpoints present in the training data. This task is particularly demanding as it usually necessitates reliable

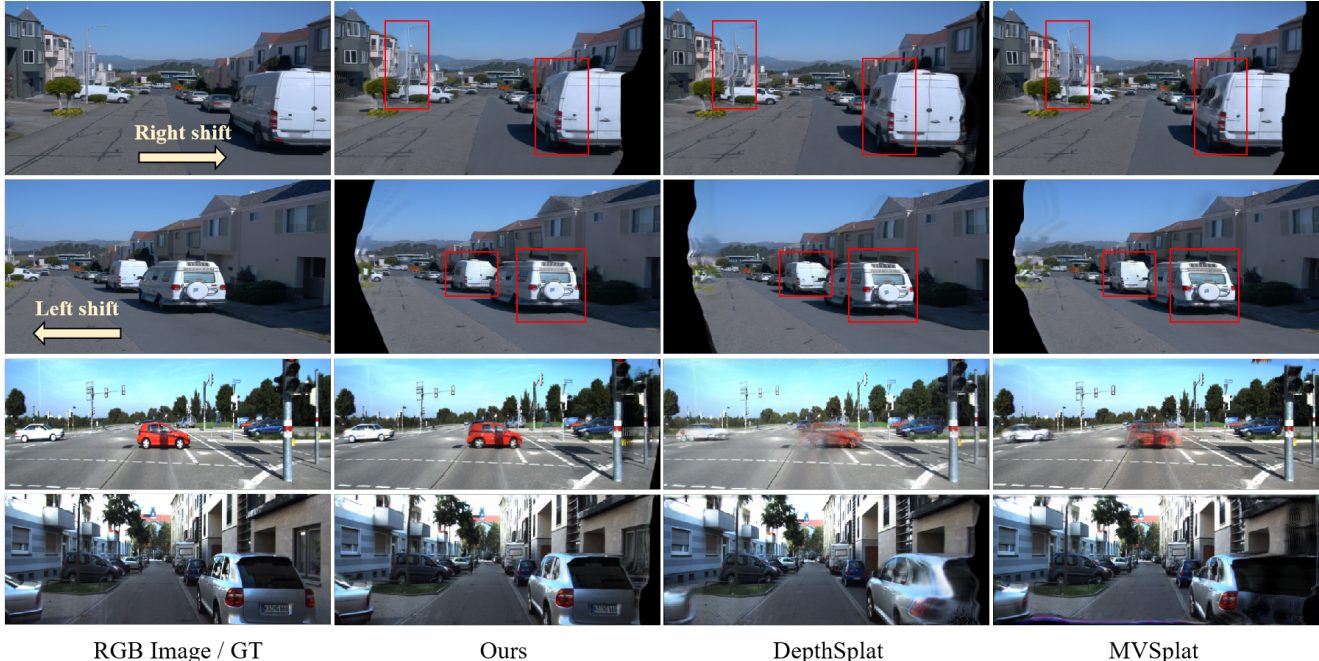


Figure 6. **Visual comparisons on view shifting.** The first two rows display the performance of right and left shifting of the given images on the Waymo dataset, whereas the last two rows report visual comparisons between the Ground Truth (GT) and shifted results. The challenging areas are marked with red rectangles. As observed, our model exhibits superior robustness under large viewpoint changes.

Method	PSNR \uparrow	SSIM \uparrow	LPIPS \downarrow
MVSplat [6]	17.25	0.554	0.381
DepthSplat [36]	12.47	0.441	0.497
Ours	17.63	0.557	0.432

Table 5. **Cross-dataset generalization.** Models trained on KITTI are directly used to test on Waymo without any further fine-tuning.

Method	PSNR \uparrow	SSIM \uparrow	LPIPS \downarrow
MVSplat [6]	14.39	0.474	0.382
DepthSplat [36]	15.07	0.452	0.377
Ours	21.81	0.770	0.184

Table 6. **Robust analysis on novel-view shifting on the KITTI dataset.** Models trained on multi-frame images are utilized directly to evaluate its capability for novel-view shifting, transitioning from the left camera to the right camera, all without additional fine-tuning. Note that our ADGaussian demonstrates superior robustness compared to prior studies on novel-view shifting.

depth estimations to handle substantial changes in viewpoint, scale, and occlusions. In this study, we further investigate the model’s robustness in view shifting. Firstly, the ground truth right camera images provided in the KITTI dataset are used to evaluate the quantitative performance of view shifting. As depicted in Table 6, our model signifi-

cantly outperforms both MVSplat and DepthSplat in zero-shot view shifting from left to right cameras. It is noteworthy that our zero-shot view shifting results are only slightly lower than our normally trained model (PSNR: 23.60, SSIM: 0.776, LPIPS: 0.164). Moreover, visual comparisons across the two datasets are presented in Figure 6. Whether shifting to the right or left, our ADGaussian exhibits exceptional overall view shifting quality on the Waymo dataset, particularly in capturing vehicle shape and intricate appearance details. Similarly, the qualitative comparisons with ground truth images on the KITTI dataset further validate the superiority of our model in view shifting.

5. Conclusion

This paper introduced a novel multi-modal framework for generalizable street scene reconstruction, demonstrating that the joint optimization of multi-modal features significantly improves both geometric and visual reconstruction quality. Additionally, we validated that our model supports zero-shot viewpoint shifting, highlighting its capabilities in generating reliable scale cues.

Limitations. Due to its reliance on single-frame input, our method’s accuracy is limited on lower-quality datasets, and its improvements in dynamic scenes are less significant than in static scenes. These issues can be addressed in future works by effectively integrating multi-frame information.

References

- [1] Reiner Birkl, Diana Wofk, and Matthias Müller. Midas v3. 1—a model zoo for robust monocular relative depth estimation. *arXiv preprint arXiv:2307.14460*, 2023. 3
- [2] Aleksei Bochkovskii, Amaël Delaunoy, Hugo Germain, Marcel Santos, Yichao Zhou, Stephan R Richter, and Vladlen Koltun. Depth pro: Sharp monocular metric depth in less than a second. *arXiv preprint arXiv:2410.02073*, 2024. 3
- [3] David Charatan, Sizhe Lester Li, Andrea Tagliasacchi, and Vincent Sitzmann. pixelsplat: 3d gaussian splats from image pairs for scalable generalizable 3d reconstruction. In *Proceedings of the IEEE/CVF Conference on Computer Vision and Pattern Recognition*, pages 19457–19467, 2024. 2
- [4] Yurui Chen, Chun Gu, Junzhe Jiang, Xiatian Zhu, and Li Zhang. Periodic vibration gaussian: Dynamic urban scene reconstruction and real-time rendering. *arXiv preprint arXiv:2311.18561*, 2023. 1, 3
- [5] Yun Chen, Jingkan Wang, Ze Yang, Sivabalan Manivasagam, and Raquel Urtasun. G3r: Gradient guided generalizable reconstruction. In *European Conference on Computer Vision*, pages 305–323. Springer, 2024. 2
- [6] Yuedong Chen, Haofei Xu, Chuanxia Zheng, Bohan Zhuang, Marc Pollefeys, Andreas Geiger, Tat-Jen Cham, and Jianfei Cai. Mvsplat: Efficient 3d gaussian splatting from sparse multi-view images. In *European Conference on Computer Vision*, pages 370–386. Springer, 2024. 2, 5, 8
- [7] Jaeyoung Chung, Jeongtaek Oh, and Kyoung Mu Lee. Depth-regularized optimization for 3d gaussian splatting in few-shot images. In *Proceedings of the IEEE/CVF Conference on Computer Vision and Pattern Recognition*, pages 811–820, 2024. 2
- [8] Andreas Geiger, Philip Lenz, and Raquel Urtasun. Are we ready for autonomous driving? the kitti vision benchmark suite. In *2012 IEEE conference on computer vision and pattern recognition*, pages 3354–3361. IEEE, 2012. 5
- [9] Huasong Han, Kaixuan Zhou, Xiaoxiao Long, Yusen Wang, and Chunxia Xiao. Ggs: Generalizable gaussian splatting for lane switching in autonomous driving. *arXiv preprint arXiv:2409.02382*, 2024. 2
- [10] Nan Huang, Xiaobao Wei, Wenzhao Zheng, Pengju An, Ming Lu, Wei Zhan, Masayoshi Tomizuka, Kurt Keutzer, and Shanghang Zhang. S3gaussian: Self-supervised street gaussians for autonomous driving. *arXiv preprint arXiv:2405.20323*, 2024. 3
- [11] Yuanhui Huang, Wenzhao Zheng, Yunpeng Zhang, Jie Zhou, and Jiwen Lu. Gaussianformer: Scene as gaussians for vision-based 3d semantic occupancy prediction. In *European Conference on Computer Vision*, pages 376–393. Springer, 2024. 2
- [12] Changjian Jiang, Ruilan Gao, Kele Shao, Yue Wang, Rong Xiong, and Yu Zhang. Li-gs: Gaussian splatting with lidar incorporated for accurate large-scale reconstruction. *IEEE Robotics and Automation Letters*, 2024. 3
- [13] Hanwen Jiang, Zhenyu Jiang, Yue Zhao, and Qixing Huang. Leap: Liberate sparse-view 3d modeling from camera poses. In *International Conference on Learning Representations*, 2023. 2
- [14] Bernhard Kerbl, Georgios Kopanas, Thomas Leimkühler, and George Drettakis. 3d gaussian splatting for real-time radiance field rendering. *ACM Trans. Graph.*, 42(4):139–1, 2023. 1
- [15] Mustafa Khan, Hamidreza Fazlali, Dhruv Sharma, Tongtong Cao, Dongfeng Bai, Yuan Ren, and Bingbing Liu. Autosplat: Constrained gaussian splatting for autonomous driving scene reconstruction. *arXiv preprint arXiv:2407.02598*, 2024. 3
- [16] Diederik P Kingma. Adam: A method for stochastic optimization. *arXiv preprint arXiv:1412.6980*, 2014. 5
- [17] Pou-Chun Kung, Xianling Zhang, Katherine A Skinner, and Nikita Jaipuria. Lihi-gs: Lidar-supervised gaussian splatting for highway driving scene reconstruction. *arXiv preprint arXiv:2412.15447*, 2024. 1
- [18] Vincent Leroy, Yohann Cabon, and Jérôme Revaud. Grounding image matching in 3d with mast3r. In *European Conference on Computer Vision*, pages 71–91. Springer, 2024. 4
- [19] Hao Li, Yuanyuan Gao, Chenming Wu, Dingwen Zhang, Yalun Dai, Chen Zhao, Haocheng Feng, Errui Ding, Jingdong Wang, and Junwei Han. Ggrt: Towards pose-free generalizable 3d gaussian splatting in real-time. In *European Conference on Computer Vision*, pages 325–341. Springer, 2024. 2, 5
- [20] Tianqi Liu, Guangcong Wang, Shoukang Hu, Liao Shen, Xinyi Ye, Yuhang Zang, Zhiguo Cao, Wei Li, and Ziwei Liu. Mvs gaussian: Fast generalizable gaussian splatting reconstruction from multi-view stereo. In *European Conference on Computer Vision*, pages 37–53. Springer, 2024. 2
- [21] Luigi Piccinelli, Yung-Hsu Yang, Christos Sakaridis, Mattia Segu, Siyuan Li, Luc Van Gool, and Fisher Yu. Unidepth: Universal monocular metric depth estimation. In *Proceedings of the IEEE/CVF Conference on Computer Vision and Pattern Recognition*, pages 10106–10116, 2024. 2
- [22] René Ranftl, Alexey Bochkovskiy, and Vladlen Koltun. Vision transformers for dense prediction. In *Proceedings of the IEEE/CVF international conference on computer vision*, pages 12179–12188, 2021. 4
- [23] Brandon Smart, Chuanxia Zheng, Iro Laina, and Victor Adrian Prisacariu. Splatt3r: Zero-shot gaussian splatting from uncalibrated image pairs. *arXiv preprint arXiv:2408.13912*, 2024. 2
- [24] Pei Sun, Henrik Kretzschmar, Xerxes Dotiwalla, Aurelien Chouard, Vijaysai Patnaik, Paul Tsui, James Guo, Yin Zhou, Yuning Chai, Benjamin Caine, et al. Scalability in perception for autonomous driving: Waymo open dataset. In *Proceedings of the IEEE/CVF conference on computer vision and pattern recognition*, pages 2446–2454, 2020. 5
- [25] Stanislaw Szymanowicz, Eldar Insafutdinov, Chuanxia Zheng, Dylan Campbell, João F Henriques, Christian Rupprecht, and Andrea Vedaldi. Flash3d: Feed-forward generalisable 3d scene reconstruction from a single image. *arXiv preprint arXiv:2406.04343*, 2024. 2
- [26] Stanislaw Szymanowicz, Christian Rupprecht, and Andrea Vedaldi. Splatter image: Ultra-fast single-view 3d reconstruction. In *Proceedings of the IEEE/CVF Conference on*

- Computer Vision and Pattern Recognition*, pages 10208–10217, 2024. 2
- [27] Jie Tang, Fei-Peng Tian, Boshi An, Jian Li, and Ping Tan. Bilateral propagation network for depth completion. In *Proceedings of the IEEE/CVF Conference on Computer Vision and Pattern Recognition*, pages 9763–9772, 2024. 6, 7
- [28] Prune Truong, Marie-Julie Rakotosaona, Fabian Manhardt, and Federico Tombari. Sparf: Neural radiance fields from sparse and noisy poses. In *Proceedings of the IEEE/CVF Conference on Computer Vision and Pattern Recognition*, pages 4190–4200, 2023. 2
- [29] Matias Turkulainen, Xuqian Ren, Iaroslav Melekhov, Otto Seiskari, Esa Rahtu, and Juho Kannala. Dn-splatter: Depth and normal priors for gaussian splatting and meshing. *arXiv preprint arXiv:2403.17822*, 2024. 2
- [30] Shuzhe Wang, Vincent Leroy, Yohann Cabon, Boris Chidlovskii, and Jerome Revaud. Dust3r: Geometric 3d vision made easy. In *Proceedings of the IEEE/CVF Conference on Computer Vision and Pattern Recognition*, pages 20697–20709, 2024. 4
- [31] Yufei Wang, Bo Li, Ge Zhang, Qi Liu, Tao Gao, and Yuchao Dai. Lrru: Long-short range recurrent updating networks for depth completion. In *Proceedings of the IEEE/CVF international conference on computer vision*, pages 9422–9432, 2023. 6
- [32] Yunsong Wang, Tianxin Huang, Hanlin Chen, and Gim Hee Lee. Freesplat: Generalizable 3d gaussian splatting towards free-view synthesis of indoor scenes. *arXiv preprint arXiv:2405.17958*, 2024. 2
- [33] Zhou Wang, Alan C Bovik, Hamid R Sheikh, and Eero P Simoncelli. Image quality assessment: from error visibility to structural similarity. *IEEE transactions on image processing*, 13(4):600–612, 2004. 5
- [34] Christopher Wewer, Kevin Raj, Eddy Ilg, Bernt Schiele, and Jan Eric Lenssen. latentsplat: Autoencoding variational gaussians for fast generalizable 3d reconstruction. In *European Conference on Computer Vision*, pages 456–473. Springer, 2024. 2
- [35] Ke Wu, Kaizhao Zhang, Zhiwei Zhang, Shanshuai Yuan, Muer Tie, Julong Wei, Zijun Xu, Jieru Zhao, Zhongxue Gan, and Wenchao Ding. Hgs-mapping: Online dense mapping using hybrid gaussian representation in urban scenes. *arXiv preprint arXiv:2403.20159*, 2024. 3
- [36] Haofei Xu, Songyou Peng, Fangjinhua Wang, Hermann Blum, Daniel Barath, Andreas Geiger, and Marc Pollefeys. Depthsplat: Connecting gaussian splatting and depth. *arXiv preprint arXiv:2410.13862*, 2024. 2, 5, 8
- [37] Yinghao Xu, Zifan Shi, Wang Yifan, Hansheng Chen, Ceyuan Yang, Sida Peng, Yujun Shen, and Gordon Wetstein. Grm: Large gaussian reconstruction model for efficient 3d reconstruction and generation. In *European Conference on Computer Vision*, pages 1–20. Springer, 2024. 2
- [38] Yunzhi Yan, Haotong Lin, Chenxu Zhou, Weijie Wang, Haiyang Sun, Kun Zhan, Xianpeng Lang, Xiaowei Zhou, and Sida Peng. Street gaussians for modeling dynamic urban scenes.(2023). 2023. 1
- [39] Lihe Yang, Bingyi Kang, Zilong Huang, Xiaogang Xu, Jiashi Feng, and Hengshuang Zhao. Depth anything: Unleashing the power of large-scale unlabeled data. In *Proceedings of the IEEE/CVF Conference on Computer Vision and Pattern Recognition*, pages 10371–10381, 2024. 3
- [40] Lihe Yang, Bingyi Kang, Zilong Huang, Zhen Zhao, Xiaogang Xu, Jiashi Feng, and Hengshuang Zhao. Depth anything v2. *arXiv preprint arXiv:2406.09414*, 2024. 2, 3
- [41] Botao Ye, Sifei Liu, Haoifei Xu, Xueting Li, Marc Pollefeys, Ming-Hsuan Yang, and Songyou Peng. No pose, no problem: Surprisingly simple 3d gaussian splats from sparse unposed images. *arXiv preprint arXiv:2410.24207*, 2024. 2
- [42] Wei Yin, Chi Zhang, Hao Chen, Zhipeng Cai, Gang Yu, Kaixuan Wang, Xiaozhi Chen, and Chunhua Shen. Metric3d: Towards zero-shot metric 3d prediction from a single image. In *Proceedings of the IEEE/CVF International Conference on Computer Vision*, pages 9043–9053, 2023. 3
- [43] Kai Zhang, Sai Bi, Hao Tan, Yuanbo Xiangli, Nanxuan Zhao, Kalyan Sunkavalli, and Zexiang Xu. Gs-irm: Large reconstruction model for 3d gaussian splatting. In *European Conference on Computer Vision*, pages 1–19. Springer, 2024. 2
- [44] Richard Zhang, Phillip Isola, Alexei A Efros, Eli Shechtman, and Oliver Wang. The unreasonable effectiveness of deep features as a perceptual metric. In *Proceedings of the IEEE conference on computer vision and pattern recognition*, pages 586–595, 2018. 5
- [45] Youmin Zhang, Xianda Guo, Matteo Poggi, Zheng Zhu, Guan Huang, and Stefano Mattoccia. Completionformer: Depth completion with convolutions and vision transformers. In *Proceedings of the IEEE/CVF conference on computer vision and pattern recognition*, pages 18527–18536, 2023. 6, 7
- [46] Cheng Zhao, Su Sun, Ruoyu Wang, Yuliang Guo, Jun-Jun Wan, Zhou Huang, Xinyu Huang, Yingjie Victor Chen, and Liu Ren. Tcgc-gs: Tightly coupled lidar-camera gaussian splatting for autonomous driving: Supplementary materials. In *European Conference on Computer Vision*, pages 91–106. Springer, 2024. 3
- [47] Shunyuan Zheng, Boyao Zhou, Ruizhi Shao, Boning Liu, Shengping Zhang, Liqiang Nie, and Yebin Liu. Gps-gaussian: Generalizable pixel-wise 3d gaussian splatting for real-time human novel view synthesis. In *Proceedings of the IEEE/CVF Conference on Computer Vision and Pattern Recognition*, pages 19680–19690, 2024. 2
- [48] Hongyu Zhou, Jiahao Shao, Lu Xu, Dongfeng Bai, Weichao Qiu, Bingbing Liu, Yue Wang, Andreas Geiger, and Yiyi Liao. Hugs: Holistic urban 3d scene understanding via gaussian splatting. In *Proceedings of the IEEE/CVF Conference on Computer Vision and Pattern Recognition*, pages 21336–21345, 2024. 1
- [49] Xiaoyu Zhou, Zhiwei Lin, Xiaojun Shan, Yongtao Wang, Deqing Sun, and Ming-Hsuan Yang. Drivinggaussian: Composite gaussian splatting for surrounding dynamic autonomous driving scenes. In *Proceedings of the IEEE/CVF Conference on Computer Vision and Pattern Recognition*, pages 21634–21643, 2024. 3